about point A takes the form

$$[(I_{Lc_x} + I_{Pc_x})\omega_x - mlv_{Lc_y} - Mz_Pv_{Pc_y}]\Big|_{t_d^-}^{t_d^+} = 0 \quad (3)$$

$$[(I_{Lc_y} + I_{Pc_y})\omega_y + mlv_{Lc_x} + M(z_Pv_{Pc_x} - hv_{Pc_z})]\Big|_{t_d^-}^{t_d^+} = 0 \quad (4)$$

$$[(I_{Lc_z} + I_{Pc_z})\omega_z + Mhv_{Pc_y}]\Big|_{t_d^-}^{t_d^+} = 0 \quad (5)$$

where only the values of the angular and linear velocity components are affected by disengagement. The pod-leg connecting point condition is expressed as

$$v_{Pc_z}(t_d^+) = v_{Lc_z}(t_d^-) - h\omega_y(t_d^+)$$

The necessary kinematic relations between leg and pod are listed in Table 1. If components of angular and linear velocity are known at t_d^-, then disengagement relations will uniquely determine all values of vehicle motion at time t_d^+.

At the end of the plane-change maneuver, engagement occurs over an infinitesimal time interval. Vehicle angular and linear momentum are conserved, and initial ballistic coordinate and velocity values at t_e^+ can be uniquely determined from conditions at t_e^-. Equating angular momentum components about point A at times t_e^- and t_e^+ gives conditions (3–5) with t_d everywhere replaced by t_e. Equating linear momentum components at times t_e^- and t_e^+ gives

$$[mv_{Lc_x} + Mv_{Pc_x}]\Big|_{t_e^-}^{t_e^+} = 0, \quad [mv_{Lc_y} + Mv_{Pc_y}]\Big|_{t_e^-}^{t_e^+} = 0$$

$$Mv_{Pc_z}|_{t_e^-} = [mv_{Lc_z} + Mv_{Pc_z}]|_{t_e^+}$$

The kinematic relations of Table 1 apply at engagement when t_d^- and t_d^+ are replaced by t_e^+ and t_e^-, respectively.

The primary objective of this analysis is to relate an initial ballistic flight plane to a new flight plane. These planes are defined by the c.m.$_v$ velocity components which lie in the XY-plane. Inertial velocity components $\dot{X}_{\text{c.m.}}(t_d^-)$, $\dot{Y}_{\text{c.m.}}(t_d^-)$, and $\dot{Z}_{\text{c.m.}}(t_d^-)$ are assumed to be given in addition to $z_P(t_d^-)$ and the Euler angles and their rates at time t_d^-. These c.m.$_v$ velocities must be converted to body-fixed coordinates before disengagement conditions can be calculated. This is done by using the well-known orthogonality transformation for Euler angles.[3] c.m.$_v$ velocity components are related to c.m.$_L$ components with the aid of Fig. 3,

$$v_{Lc_x} = v_{cm_x} - (z_c - l)\omega_y \quad (6)$$

$$v_{Lc_y} = v_{cm_y} - x_c\omega_z + (z_c - l)\omega_x \quad (7)$$

$$v_{Lc_z} = v_{cm_z} + x_c\omega_y \quad (8)$$

where

$$x_c = \zeta h/\eta, \; z_c = [\zeta(z_P - l)/\eta] + l$$

$$\zeta = M\eta/(M + m), \; \eta = [(z_P - l)^2 + h^2]^{1/2}$$

Values given by these expressions are used with disengagement conditions to convert c.m.$_v$ components into c.m.$_L$ and c.m.$_P$ components. At the subsequent engagement event, values of c.m.$_v$ velocity components must be obtained in terms of the inertial frame. First, these components are calculated in body-fixed coordinates from components of the c.m.$_L$ velocity at time t_e^+ by solving Eqs. (6–8). Then another orthogonality transformation is performed to obtain inertial coordinates. The expressions presented to this point completely describe the dynamical state of this vehicle model in the interval $t_d^- \leq t \leq t_e^+$. Given c.m.$_v$ velocity components and angular state with z_P at time t_d^-, these relationships can be solved to generate the entire state of vehicle dynamics at time t_e^+. Thus,

$$\delta(t_e^+) = \tan^{-1}[\dot{Y}_{\text{c.m.}}(t_e^+)/\dot{X}_{\text{c.m.}}(t_e^+)]$$

The desired value of plane change is just the difference of this and the initial plane angle $\delta(t_e^-)$.

Conclusions

The general dynamical motion of a lunar hopping vehicle is, at best, extremely complex. Only one simplified aspect of the dynamics problem has been considered here, development of the equations of motion for the plane-change maneuver. A general solution has not yet been discovered, but specialized numerical results are obtainable for given initial conditions. In order to design a navigational computer and control system for such a vehicle, the plane-change problem must be completely solved. This will require a considerable amount of effort beyond the present state of knowledge.

References

[1] Seifert, H. S., "The Lunar Pogo Stick," *Journal of Spacecraft and Rockets*, Vol. 4, No. 7, July 1967, pp. 941–943.

[2] Kaplan, M. H. and Seifert, H. S., "Hopping Transporters for Lunar Exploration," *Journal of Spacecraft and Rockets*, Vol. 6, No. 8, Aug. 1969, pp. 917–922.

[3] Goldstein, H., *Classical Mechanics*, Addison-Wesley, Reading, Mass., 1950, pp. 14–18, 107–109, 132–134, 149.

A Guarded Disk-Type Sample Emissometer

JOHN G. ANDROULAKIS*
Grumman Aircraft Engineering Corporation, Bethpage, N. Y.

Nomenclature

P = power applied to the sample heater
E = voltage drop across the sample heater
I = current
A_s = total radiating area of the two sample disks
σ = Stefan-Boltzman constant
T_s, T_0 = sample and cold cavity temperatures
ϵ_s = total hemispherical emittance of the sample
ϵ_n = total normal emittance
α_s = absorptance of the sample for energy radiated by the cold cavity walls
q = heat flow; q_l, heat leak through the lead wires; q_g, through the residual gas; q_r, net radiation loss through the edge of the sample and sample heater to the guard ring and cold cavity
w = mass
c = heat capacity
$\dot{T}$ = derivative of temperature with respect to time

Introduction

KNOWLEDGE of the total hemispherical emittance ϵ_s of materials at satellite temperature ranges is important for the thermal design of space or space simulation systems. Calorimetric methods for ϵ_s measurement are based on either the transient or the steady-state modes. When the transient mode is used, the accuracy of the measured ϵ_s depends upon accurate knowledge of the heat capacity, $c = c(T)$, of the specimen. Very often the specimen consists of a relatively thick coating on a thin metal substrate, in which case transient ϵ_s

Presented as Paper 69-600 at the AIAA 4th Thermophysics Conference, San Francisco, Calif., June 16–18, 1969; submitted October 13, 1969; revision received December 19, 1969. This effort was performed under the sponsorship of the Grumman Aircraft Engineering Corporation, Advanced Development Program. Project AP 04-02.

* Senior Thermodynamics Engineer. Member AIAA.

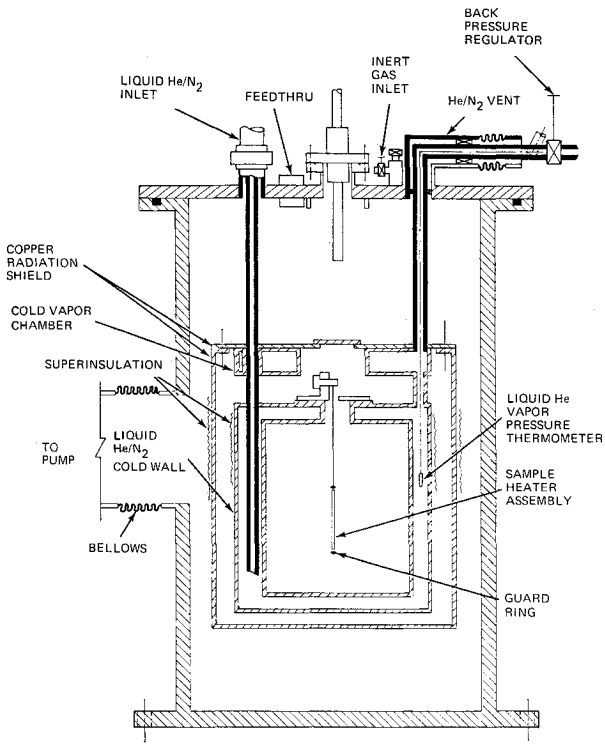

Fig. 1 Schematic drawing of the apparatus.

measurements, requiring measurement of wc of the specimen, become more complicated.[1] The steady-state mode, in general, comprises two classes of specimen geometry: resistance-heated, long, slender samples,[2] and disk-type samples (or squares) heated by an electrical element or by radiation. The disk type may be used in a symmetrical arrangement[3,4] consisting of two sample disks (or squares) with a heater between, or in systems comprising only one sample disk[5] with fundamental variation in system conception.

Although the symmetrical arrangement of the disk type seems more practical, the design of such a system for accurate emittance measurements actually is difficult because of the inherent errors associated with the calorimetric technique, particularly at low temperatures where the energy fluxes involved are very small. Some major sources of errors contributing directly to the heat measurement accuracy are: a) radiation losses from the edge (since the edge must be thick to incorporate an internal heater); b) heat leaks through the thermocouple wires, power leads, and sample holder (if other than the lead wires); and c) the small size of the sample-heater mass, required so as to rapidly reach an equilibrium temperature with negligible internal energy changes at the moment of measurement. Furthermore, since low ϵ samples require large areas exposed to radiation (consistent with accurate electric power measurements), obtaining a uniform sample surface temperature T_s is a problem.

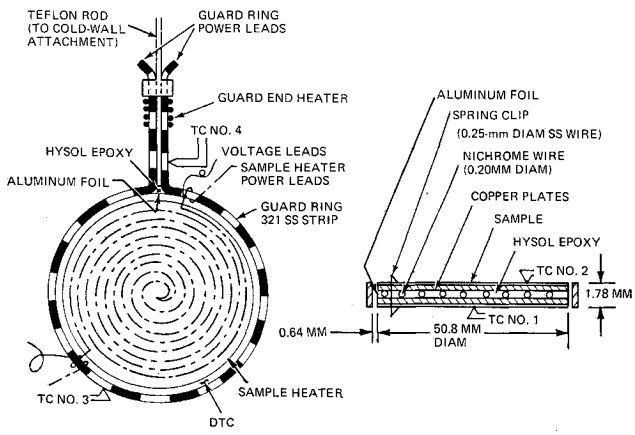

Fig. 2 Guard ring and sample heater assembly.

This Note describes an improved symmetric disk arrangement capable of measuring ϵ_s in the 88°K to 420°K (−300°F to +300°F) temperature range. Its main feature is the holding of the sample heater assembly concentric to an isothermal guard heater ring, the inner surface of which is kept at the same temperature as the sample heater edge. The addition of the isothermal guard heater ring and the development of sample heaters of small mass and uniform surface temperature minimizes most of the errors associated with the calorimetric technique. Close temperature control is achieved by the use of a feedback temperature control loop, which makes the operation of the system very simple.

Experimental Arrangement

The basic system (Figs. 1 and 2) consists, primarily, of the guard ring-sample heater assembly, a cold wall cavity, and an external vacuum chamber. The apparatus is essentially constructed of stainless steel. The cold wall cavity may be cooled to either liquid N_2 or liquid He temperature using bath-type refrigeration. A copper radiation shield is conduction-cooled by thermal contact with an upper cold vapor chamber through which the exhausted cold gas passes. The guard ring-sample heater assembly is suspended inside the cold wall cavity by means of a teflon rod which is held at the other end by a clamp thermally grounded to the cold cavity. To minimize interreflections between sample and surroundings, the inner surface of the cold cavity is covered with roughened black epoxy paint and is of an area much larger than the sample area exposed to radiation (ratio of areas >22). In addition, the sample is suspended eccentrically to the cavity axis of symmetry to avoid energy returns from the eventual specularity of the black paint at low temperatures.

The guard heater ring, Fig. 2, consists of a resistance-heated, 321 stainless steel strip, 0.8-mm (0.031-in.) thick by 1.78 -mm wide. For high-ϵ samples, the guard heater ring may be a sheathed nichrome wire. The ring is completed on the top by filling the small gap with hysol (epoxy cement) covered with aluminimized mylar tape at the inner ring surface. A guard end heater is provided for additional heating of both ends of the guard heater ring.

The sample heater, Fig. 2, is made of 0.2-mm diam nichrome wire wound uniformally, in a spiral form, on a thin layer of hysol epoxy cement, and sandwiched between two thin 50.8-mm-diam copper plates. The choice of the diameter and length of the heating wire was influenced by the maximum number of coil turns compatible with temperature uniformity and accurate electric power measurements. Various guard ring-sample heater assemblies were constructed with sample heater thickness ranging from 0.76 to 1.04 mm, to accommodate various sample thicknesses. The total sample heater thickness, after attachment of the two sample disks, is approximately equal to the guard ring width.

The net radiation loss from the sample heater edge is minimized by covering the edge surface with aluminum foil and making the average gap between sample heater and ring 0.635 mm. The sample heater is suspended from the guard ring by means of the two sample-heater power leads, which come from opposite sides of the heater and hold it firmly inside the ring. These sections of the power leads are warmer than the sample heater and ring, but introduce an insignificant error to the power measurement (less than 0.1% with the voltage leads attached to the sample heater coil leads at the guard ring). Heat conducted through the thermocouple wires is minimized by thermally grounding a sufficient length of wire around the guard heater ring. For the thermocouple wires attached to the sample, a 76-mm length bare wire is left between junction and guard heater ring.

The cold-wall temperature is measured by means of a vapor pressure thermometer near liquid He temperature and by means of copper-constantan thermocouples above liquid N_2 temperature. The temperature of the sample and guard ring is measured with 0.051-mm- or 0.127-mm-diam calibrated copper-constantan thermocouples, whose junctions are either welded to the sample or, when welding is not possible, buried in the sample and secured by a low-temperature cement. The use of thermocouples of lower thermal conductivity wires, such as chromel vs constantan, would reduce the heat leak through the wires.

The thermocouple output voltage is measured with a Leeds and Northrup type K-3 potentiometer. Power to the sample heater, which is supplied by a variable transformer, is calculated from sample heater current (measured from the voltage drop across a standard resistor) and voltage drop measured by a Fluke differential d.c.-a.c. voltmeter model 987AB). The differential temperature between the sample heater edge and the guard heater ring is controlled by a closed feedback control loop using a three-mode control action similar to that described in Ref. 2. The power input to the guard end heater is supplied by a variable transformer.

The sample consists of two disks, each of 50.1-mm diam firmly secured against the two copper face plates of the heater by means of 3 or 4 spring clips which touch only the two samples. A thin layer of high-conductivity grease is used between mating surfaces to provide better thermal contact. The sample thickness is kept small, compatible with the small temperature gradient across the sample and consequently smaller net radiation loss through the sample edge.

Experimental Procedure

The temperature of one of the samples (Fig. 2), is measured at the center, and that of the other at 6.35 mm from the edge. Usually, both samples are isothermal, and essentially at the same temperature. The temperature of the guard heater ring is measured at the top and bottom.

During operation, the main heater, which supplies current to the sample heater, is turned on, with subsequent operation of the feedback control loop which brings the temperature of the lower portion of the guard heater ring to the same value as that of the sample heater. The guard end heater is then turned on to bring the temperature of the upper portion of the ring to the same value as that of the lower portion. In order to use the guard end heater to make the guard heater ring isothermal, the two ends of the ring must be at a lower temperature than the center during resistance heating. To minimize heat leakage to the ends, the guard heater ring is supported by a teflon rod attached to the cold wall; all lead wires are thermally grounded to some extent around the cold pipes. The procedure for making the ring isothermal is similar to that described in Ref. 2 for obtaining an isothermal sample in the resistance-heated, long, slender sample calorimetric technique.

To shorten test duration, dry helium gas is introduced to cool the sample rapidly to the desired temperature. Measurements are made in a vacuum between 1.33×10^{-5} and 1.33×10^{-6} N/m^2 (10^{-7} to 10^{-8} torr).

Emittance and Error Determination Technique

Total hemispherical emittance ϵ_s is determined from measurements of the power (EI) input to the sample heater, T_s, T_0, and the total radiating area A_s of the sample. The simplified heat balance equation is:

$$P = EI = \epsilon_s A_s \sigma (T_s^4 - T_0^4) \qquad (1)$$

Corrections due to inherent errors of the apparatus are not applied to the ϵ_s calculated from Eq. (1). A maximum possible experimental error is evaluated as follows. Assuming no inter-reflections between sample and cold wall, the most general heat balance expression for the sample is:

$$P = \epsilon_s \sigma A_s (T_s^4 - T_0^4) - \Delta\alpha_s A_s \sigma \epsilon_s T_0^4 + q + wc\dot{T} \qquad (2)$$

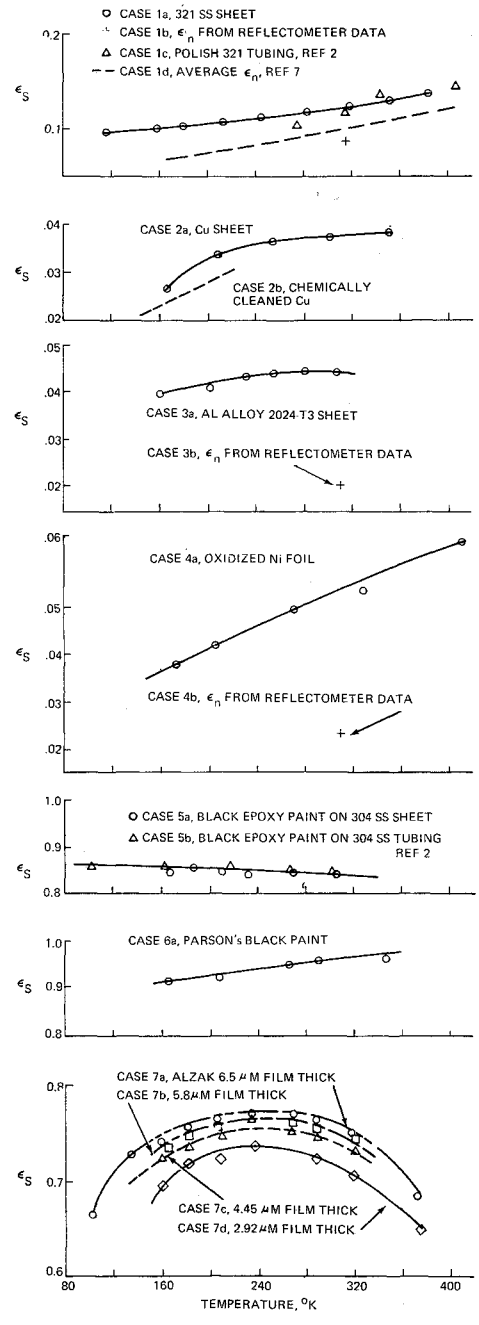

Fig. 3 Total hemispherical emittance of some metals and coatings.

where w, c and $\dot{T}$ refer to the sample heater assembly, $\alpha_s = \epsilon_s + \Delta\alpha_s$, and $q = q_l + q_q + q_r$. Equation (2) gives, after differentiation, an equation which can be simplified to the following form by setting $q = \dot{T} = \Delta\alpha_s = 0$, since Eq. (2) is reduced to Eq. (1) under these conditions:

$$\frac{\delta\epsilon_s}{\epsilon_s} = \underbrace{\frac{\delta A_s}{A_s}}_{(a)} + \underbrace{\left(\frac{4T_s^4}{T_s^4 - T_0^4}\frac{\delta T_s}{T_s} + \frac{4T_0^4}{T_s^4 - T_0^4}\frac{\delta T_0}{T_0}\right)}_{(b)} + \underbrace{\frac{\delta p + \delta q + wc\delta\dot{T}}{\epsilon_s A_s \sigma (T_s^4 - T_0^4)}}_{(c)} + \underbrace{\frac{\delta\Delta\alpha_s T_0^4}{\epsilon_s (T_s^4 - T_0^4)}}_{(d)} \qquad (3)$$

In Eq. (3), term (3a) accounts for area measurement error, term (3b) for temperature measurement errors, term (3c) for heat measurement errors, and term (3d) for nongray error.

An error analysis based on the technique reported in Refs. 2 and 6 and on observations made during the tests reveals a

Table 1 Error summary

Source	Error, $\delta\epsilon_s/\epsilon_s$% 88°K (−300°F)	420°K (+300°F)	Remarks
Sample area measurement: $4\frac{\delta D}{D}$ [term (a) of Eq. (3)]	0.4	0.4	0.1% on diameter
Temperature measurement: [term (b) of Eq. (3)]	2.5	1.1	Based on $\delta T_s = 0.57$°K at $T = 88$°K and on $\delta T_s = 1.11$°K at $T_s = 420$°K
Power measurement: $\frac{\delta E}{E} + \frac{\delta I}{I}$	1	1	
Heat leak through the lead wires: $\frac{\delta q_l}{P}$	$\frac{0.28}{\epsilon_s}$	$\frac{0.003}{\epsilon_s}$	Based on 3 Cu-Con thermocouples of 0.127 mm diam and a temperature gradient of 2.2°K/m at 88°K and of 11°K/m at 420°K
Gas conduction: $\delta q_g/P$	$\frac{0.036}{\epsilon_s}$	$\frac{0.0003}{\epsilon_s}$	Based on a vacuum pressure of 1.33×10^{-5} N/m² (10^{-7} torr)
Radiation loss through the sample heater edge: $\delta q_r/P$	$\frac{0.05}{\epsilon_s}$	$\frac{0.05}{\epsilon_s}$	
Nonsteady state: $wc\,\delta\dot{T}/P$	$\frac{0.09}{\epsilon_s}$		Combined mass of heater and two copper substrates disk; $\dot{T} = 0.006$°K/hr
Nongray error [term (d) of Eq. (3)]	≈0 (Cavity at liquid He temp.)	$0.03\frac{\delta\Delta\alpha_s}{\epsilon_s}$	At $T_s = 172$°K and cavity at liquid N_2 temp. $\frac{\delta\epsilon_s}{\epsilon_s} = 4.55\frac{\delta\Delta\alpha_s}{\epsilon_s}$ %

maximum uncertainty on the experimental emittance value of 12% at 88°K and 3.5% at 420°K, for low emittance samples; and a value of 5% at 88°K and 2.5% at 420°K, for high emittance samples. A summary of the various contributions to the total error is shown in Table 1.

Table 2 Sample description

Key	Case	Description
0	1a	321 S.S. sheet, surface finish: 0.64 μm(25 μin.)
+	1b	ϵ_η of sample 1a, calculated from heated cavity reflectometer data
△	1c	High polished 321 S.S. tubing from Ref. 2
...	1d	Average ϵ_η of many polished samples of 321 S.S. strip from Ref. 7
0	2a	Copper sheet, comm. surface finish: 0.25 μm (10 μin.) cleaned with soap and water
...	2b	Copper chemically cleaned from Ref. 5
0	3a	Aluminum alloy 2024-T3 sheet, Surface finish: 0.64 μm (35 μin.)
+	3b	ϵ_η of sample 3a, calculated from heated cavity reflectometer data.
0	4a	Nickel 200 foil, 0.0127 mm thick oxidized at 500°K (slightly crinkled)
+	4b	ϵ_η of sample 4a, calculated from heated reflectometer data
0	5a	Grumman black epoxy paint. Two layers of No. 1019 topcoating on one layer of No. 2012 undercoating applied to 304 S.S. sheet. Over-all film thickness, 0.051 mm.
△	5b	Grumman black epoxy paint. Two layers of No. 1019 topcoating on one layer of No. 1020 clear epoxy, applied to 304 S.S. tubing. Over-all film thickness, 0.048 mm from Ref 2.
0	6a	Parson's black paint. Two layers of optical black lacquer topcoating on one layer of optical black lacquer undercoating applied to 321 S.S. sheet. Over-all film thickness, 0.051 mm.
		Anodized thickness, μm (mil)
0	7a	6.5 (0.255) Alzak (SI grade lighting sheet
□	7b	5.8 (0.228) anodized high purity alumi-
△	7c	4.45 (0.175) num clad on commercially
◇	7d	2.92 (0.115) pure aluminum substrate)

Experimental Results

Some of the experimental results are presented in Fig. 3 and are coded in Table 2. The emittance values below 170°K, of 321 stainless steel, case 1a, and Alzak, case 7a, were obtained with the cold cavity kept at liquid He temperature. The other emittances were obtained with the cavity kept at the liquid N_2 temperature. In some cases the ϵ_s obtained is compared with the ϵ_s or ϵ_n obtained by other techniques. For 321 stainless steel case 1a, results compare well, since the ϵ_n from Ref. 7 corresponds to a better surface finish. The ϵ_s values, case 2b of the chemically cleaned copper, from Ref. 5, are somewhat lower than those of the mechanically polished copper obtained with the apparatus herein described. Cases 3a and 4a show values of ϵ_n for low-ϵ_s samples, to be $\sim 0.5\epsilon_s$. According to the theory, ϵ_η/ϵ_s should be somewhat larger ($\sim$0.75). However, the samples tested are not ideal in the sense of surface cleanness, surface roughness, and imperfections behind the surface. Also, the disagreement is partially due to the errors associated with the two measuring techniques. Small percentage errors in reflectance measurements of low ϵ_s samples can result in large percentage errors in ϵ_s. Moreover, much larger radiating areas are involved in calorimetric measurements showing better the effect of large-scale surface irregularities. Emittance values of the black epoxy paint, case 6a, compare well with those obtained with the apparatus described in Ref. 2. Case 6 of Fig. 3 shows the ϵ_s of Parson's black paint; previously obtained values were ~5% lower because of slight flakes, and cracks developed by the paint during the test. Case 7 shows that the ϵ_s of Alzak increases with anodized thickness, but this increase becomes less significant at high anodized thicknesses.

Conclusions and Recommendations

The novel experimental arrangement used and the care and attention given in the construction of the system enabled the calorimetric technique, at steady state, to be successfully applied to the determination of the total hemispherical emittance of samples, in the form of disks, at low temperatures. The system is practical and, for experienced personnel, inexpensive to operate. In the future a second temperature feedback control loop will be used to monitor the power input to

the guard ring end heater. This should result in even better system performance. In addition, the upper temperature limit may be extended by selecting materials of higher heat resistance for the construction of the guard ring and sample heater.

References

[1] Makarounis, G., "Heat Capacity by the Radiant Energy Absorption Technique," *AIAA Progress in Astronautics and Aeronautics Series: Thermophysics of Spacecraft and Planetary Bodies*, Vol. 20, edited by G. B. Heller, Academic Press, New York, 1967, pp. 203–218.

[2] Androulakis, J. G., "Development and Test of a Low to Moderately High-Temperature Emissometer," *AIAA Progress in Astronautics and Aeronautics Series: Thermophysics of Spacecraft and Planetary Bodies*, Vol. 20, Edited by G. B. Heller, Academic Press, New York, 1967, pp. 151–176.

[3] Fussell, W. B. and Triolo, J. J., "A Dynamic Thermal Vacuum Technique for Measuring the Solar Absorption and Thermal Emitance of Spacecraft Coatings," *Measurement of Thermal Radiation Properties of Solids*, NASA SP-1, 1963.

[4] Gordon, G. D. and London, A., "Emittance Measurements at Satellite Temperatures," *Measurement of Thermal Radiation Properties of Solids*, NASA SP-31, 1963.

[5] Caren, R. P., "Low-Temperature Emittance Determinations," *AIAA Progress in Astronautics and Aeronautics Series: Thermophysics and Temperature Control of Spacecraft and Entry nautics Series: Thermophysics and Temperature Control of Space-Vehicles*, Vol. 18, edited by G. B. Heller, Academic Press, New York, 1966, pp. 61–74.

[6] Nelson, K. E. and Bevans, J. T., "Errors of the Calorimetric Method of Total Emittance Measurements," *Measurement of Thermal Radiation Properties of Solids*, NASA SP-31, 1963.

[7] Wood, W. D., Deem, H. W., and Lucks, C. F., "Thermal Radiation Properties of Selected Materials," Rept. 177, Nov. 1962, Defense Metals Information Center, Battelle Memorial Institute.

Planetary Trajectory Handbooks for Mission Analysis

SUSAN NORMAN*

NASA Ames Research Center, Mission Analysis Division, Moffett Field, Calif.

A COMPREHENSIVE set of trajectory handbooks (Parts 6–9) has been added to the NASA *Planetary Flight Handbook*.[1] They are specifically designed to be of use in mission or system studies and therefore include parameters such as planetary lighting conditions, Saturn ring passage conditions, and communication distances in addition to the relevant trajectory parameters. They cover opportunities from the mid-1970s to the mid-1980s for Mercury and the outer planets and to the end of the century for Mars (see Table 1) and they include general discussions of the missions, contour charts, and related information.

The titles of the new parts are: Part 6, *Mars Stopover Missions Using Venus Swingbys*†; Part 7, *Direct Trajectories to Jupiter, Saturn, Uranus, and Neptune*‡; Part 8, *Jupiter Swingby Missions to Saturn, Uranus, Neptune, and Pluto*,‡ and Part 9 (to be published), *Direct and Venus Swingby Trajectories to Mercury*.‡ Supplements containing the tabular data for Parts 6, 7, and 8 are bound separately from the descriptive sections and are available from the Technical Information Division, NASA Ames Research Center, Moffett Field, Calif. The descriptive sections are available from the Superintendent of Documents, U.S. Government Printing Office, Washington, D. C. Both the descriptive section and the tabular data for Part 9 are bound in one volume which is also available from the Superintendent of Documents.

To facilitate the use of the trajectory data by computers, magnetic tapes, which contain the tabular data used in the handbooks, have been prepared. Descriptions of these tapes and instructions for obtaining them are given in the descriptive section of each part.

Received December 24, 1969.

* Research Scientist, Office of Advanced Research and Technology.

† Prepared under contract for NASA by Douglas Aircraft, Contract NAS 2-4175.

‡ Prepared under contract for NASA by General Dynamics/Fort Worth, Contract NAS 2-4982.

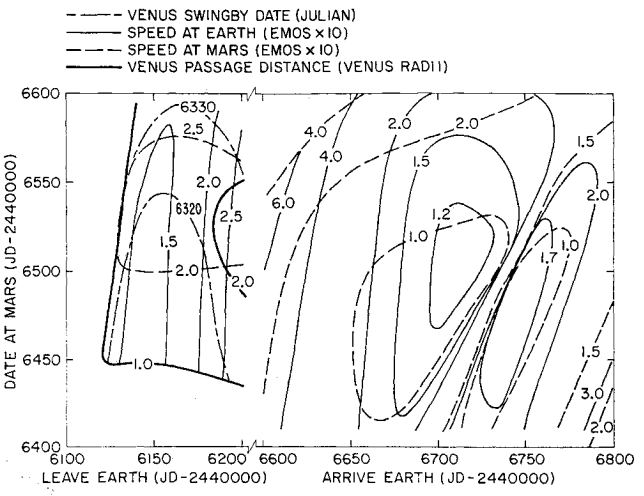

Fig. 1 Mars stopover mission using Venus swingby (1986).

Part 6

This Handbook contains data for Mars round trip missions with 0, 30, and 60 day stopovers, for which the trajectory data are contained in Supplements A, B, and C, respectively. These stopover times were selected because they encompass the region of reasonable stay times for the swingby mode and illustrate the effect of stopover time on mission parameters. Only unpowered Venus swingby missions are included in Part 6, since oneway direct trajectories to and from Mars (and also Venus) are summarized in the previously published parts 1–3.[1] The trajectory data are presented chronologically and are organized by holding stopover time, total mission duration, and Mars arrival date constant while varying Earth departure date. Next, the Mars arrival date is varied, followed by the mission duration.

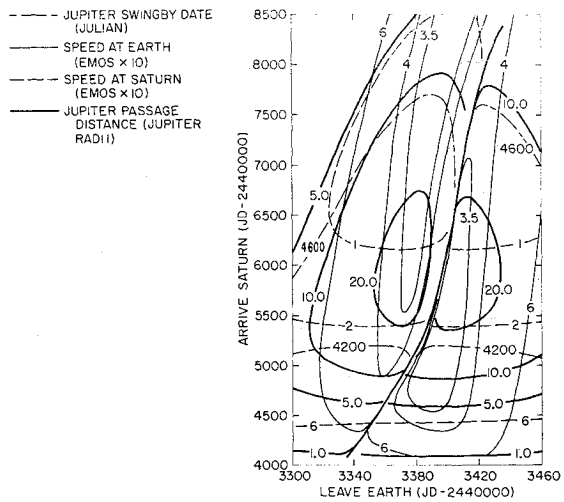

Fig. 2 Saturn mission using Jupiter swingby (1977).